Computational and Structural Biotechnology Journal 21 (2023) 2137–2146

Contents lists available at ScienceDirect

Computational and Structural Biotechnology Journal

journal homepage: www.elsevier.com/locate/csbj

Structural basis for the inhibitory mechanism of auranofin and gold(I) analogues against *Pseudomonas aeruginosa* global virulence factor regulator Vfr

Yingdan Zhang [a,b,1,2], Bing Liang Alvin Chew [c,d,e,1,3], Jing Wang [b], Mingjun Yuan [e,f], Joey Kuok Hoong Yam [e], Dahai Luo [c,d,*,4], Liang Yang [a,b,e,**,5]

[a] *Shenzhen Third People's Hospital, The Second Affiliated Hospital of Southern University of Science and Technology, National Clinical Research Center for Infectious Disease, Shenzhen 518112, China*
[b] *School of Medicine, Southern University of Science and Technology, Shenzhen 518055, Guangdong, China*
[c] *Lee Kong Chian School of Medicine, Nanyang Technological University, Singapore 636921*
[d] *NTU Institute of Structural Biology, Nanyang Technological University, EMB 06-01, 59 Nanyang Drive, 636921, Singapore*
[e] *Singapore Centre for Environmental Life Sciences Engineering (SCELSE), Nanyang Technological University, Singapore*
[f] *Guanghua Science and Technology Research Institute (Guangdong) Co., Ltd, China*

ARTICLE INFO

Article history:
Received 19 August 2022
Received in revised form 9 March 2023
Accepted 11 March 2023
Available online 13 March 2023

Keywords:
Antimicrobial
Virulence
Pseudomonas
Vfr
Auranofin
Gold(I) analogues

ABSTRACT

Pseudomonas aeruginosa is a leading cause of hospital-acquired infections. Treatment of *P. aeruginosa* infections is difficult given its multiple virulence mechanisms, intrinsic antibiotic resistance mechanisms, and biofilm-forming ability. Auranofin, an approved oral gold compound for rheumatoid arthritis treatment, was recently reported to inhibit the growth of multiple bacterial species. Here, we identify *P. aeruginosa*'s global virulence factor regulator Vfr as one target of auranofin. We report the mechanistic insights into the inhibitory mechanism of auranofin and gold(I) analogues to Vfr through structural, biophysical, and phenotypic inhibition studies. This work suggests that auranofin and gold(I) analogues have potential to be developed as anti-virulence drugs against *P. aeruginosa*.

1. Introduction

Pseudomonas aeruginosa (*P. aeruginosa*, *Pa*) is an opportunistic Gram-negative pathogen that causes a wide range of infections with high morbidity and mortality, particularly among individuals with compromised immune systems and those with cystic fibrosis [1]. *P. aeruginosa*'s emergence as a nosocomial pathogen is largely attributed to its multiple virulence mechanisms, intrinsic antibiotic resistance mechanisms, and biofilm-forming ability. This makes it a top priority for the development of novel antimicrobial drugs [2].

The virulence factor regulator (Vfr) has proved to be a promising drug target for *Pa* given its central role in controlling virulence and pathogenicity [3]. Vfr is a close homolog of the structurally well-characterized cyclic adenosine monophosphate (cAMP) receptor protein (CRP) of *Escherichia coli* (*E. coli*, *Ec*) [4]. It is a 24 kDa homodimer belonging to the winged-helix family of transcription factors. The N-terminal domain of Vfr contains a primary high-affinity cAMP binding site, while the C-terminal domain contains a secondary low-affinity cAMP binding site adjacent to the helix-turn-helix motif that binds to DNA [5]. Structural study of Vfr further identified that its N-terminal residues may play a unique role in *Pa* pathogenesis that cannot be recapitulated by the CRP complemented Vfr-deficient strain [6]. Vfr regulates approximately 200 genes in *Pa* [7], including those involved in (i) the quorum sensing (QS) [8] which controls the production of virulence factors such as elastase

* Corresponding author at: Lee Kong Chian School of Medicine, Nanyang Technological University, 636921, Singapore.
** Corresponding author at: Shenzhen Third People's Hospital, The Second Affiliated Hospital of Southern University of Science and Technology, National Clinical Research Center for Infectious Disease, Shenzhen 518112, China.
E-mail addresses: Luodahai@ntu.edu.sg (D. Luo), yangl@sustech.edu.cn (L. Yang).
[1] Co-first authors.
[2] 0000-0002-7328-154X.
[3] 0000-0002-2748-9366.
[4] 0000-0001-7637-7275.
[5] 0000-0002-2362-0128.

https://doi.org/10.1016/j.csbj.2023.03.013

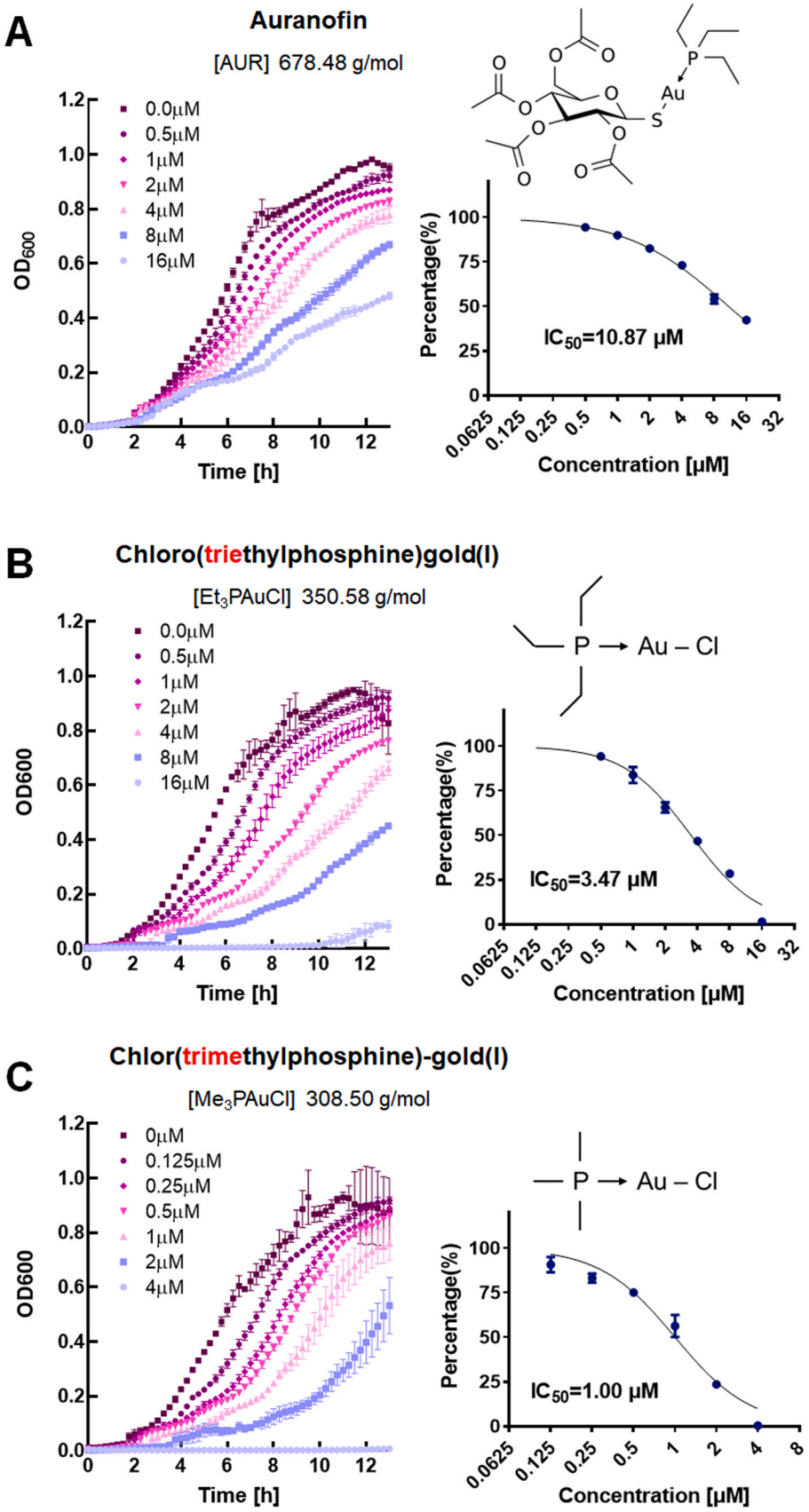

Fig. 1. Dose-dependent *Pa* growth inhibition in the presence of (A) auranofin, (B) chloro(triethylphosphine)gold(I) and (C) chloro(trimethylphosphine)gold(I). IC_{50} was calculated and listed in the figures; respectively.

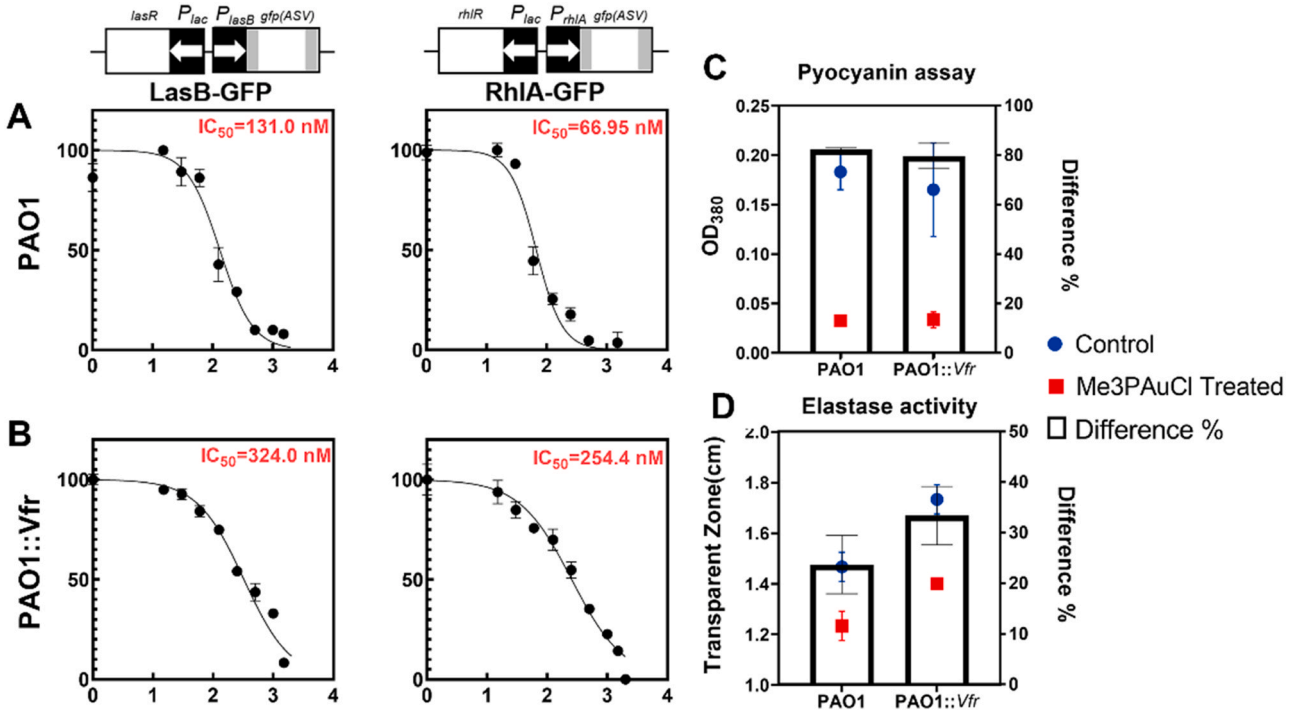

Fig. 2. Me_3PAuCl inhibits Vfr-regulated quorum sensing and virulent factors in PAO1 wild type and Vfr-overexpressed strain. (**A**) Me_3PAuCl inhibits *las* and *rhl* systems of PAO1 with IC_{50} values of 131 nM and 66.95 nM, respectively. (**B**) Me_3PAuCl inhibits *las* and *rhl* systems of PAO1::*vfr* with IC_{50} values of 324.0 nM and 254.4 nM; respectively. (**C**) Me_3PAuCl (1 μM) inhibits the pyocyanin production in both PAO1 and PAO1::*vfr*. (**D**) Me_3PAuCl (1 μM) inhibits the elastase activities in both PAO1 and PAO1::*vfr*.

[9]; (ii) the type III secretion system that can be activated by glutathione [10] and mediates bacterial cytotoxicity to host cells [11]; and (iii) the type IV pilus (TFP) formation which controls the twitching motility [12]. Given the importance of Vfr in regulating these key virulence mechanisms, further structural studies of Vfr-ligand interactions can help to elucidate its function and validate its role as a potential target for development of antimicrobial drugs.

A number of repurposing projects reported that Auranofin, an FDA-approved antirheumatic agent**,** exhibits potent antimicrobial activities and can synergize with antibiotics against a broad spectrum of pathogens [13–16]. Auranofin [2,3,4,6-tetra-o-acetyl-L-thio-b-D-glycopyranp-sato-S-(tri-ethyl-phosphine)-gold] is a gold(I) compound with phosphine and thiol ligands in a linear arrangement. It is a prodrug with the acetylated thiosugar acts as a carrier that is hydrolyzed upon transfer across cell membranes, releasing the pharmacologically active cationic fragment $[Au(PEt_3)]+$ [17,18]. The putative mechanism of action hinges on the release of its monovalent gold, Au(I), and binding to a protein target via the thiol ligand which has a high affinity for thiol and selenol groups, to form stable adducts. Interestingly, there are five cysteine residues on Vfr in the thiol state that modulate the expression of virulent factors [10]. Therefore, we hypothesize that both auranofin and gold(I) analogues with varied thiol and/or phosphine ligands may be able to target these cysteine residues of Vfr and reduce its ability to regulate key virulence mechanisms.

In this study, we examined the inhibitory effects of Vfr by auranofin and two simple gold-phosphine compounds, namely Chloro (triethylphosphine)gold(I) (Et_3PAuCl) and Chloro(trimethylphosphine)gold(I) (Me_3PAuCl). We further evaluated the crystal structures of Vfr both alone and in complex with these gold(I) analogues. Our results demonstrated the following properties of auranofin and the two simple gold-phosphine compounds as Vfr inhibitors: [1] Et_3PAuCl and Me_3PAuCl, without the thiosugar ligand, are more effective in inhibiting *Pa* growth than auranofin; [2] Au binding at Cys38 of Vfr potentially alters the primary cAMP binding pocket; [3] Au binding at Cys183 of Vfr clashes with its binding to the DNA backbone at the C-terminal domain; [4] Me_3PAuCl effectively inhibits *Pa*'s QS systems through Vfr. Altogether, this work provides important mechanistic insights into Vfr inhibition by gold compounds, highlighting their therapeutic potential against *Pa* infections.

2. Results and discussion

2.1. Antimicrobial activity of gold(I) analogues against Pa growth

We investigated the potential antimicrobial activity of gold(I) analogues against *Pa* by determining their minimal inhibition concentration (MIC) and minimal bactericidal concentration (MBC) on PAO1 strain, and comparing their effects with auranofin (Table S1). Our results revealed that the two simple gold compounds, Et_3PAuCl and Me_3PAuCl, demonstrated potent inhibition of PAO1 growth, with MIC (defined as IC_{90}) values of 20.57 μM and 3.97 μM, respectively. And the IC_{50} values of Et_3PAuCl and Me_3PAuCl were 3.47 μM and 1.00 μM, respectively (Fig. 1). In contrast, the MIC and IC_{50} value of auranofin was approximately 130.3 μM and 10.87 μM, indicating that both gold-compounds are 3–10 times more effective at inhibiting *Pa* growth. Notably, Et_3PAuCl closely resembles the active form of auranofin, while Me_3PAuCl exhibits higher reactivity.

The growth inhibition effects by auranofin and Et_3PAuCl on both Gram-positive and Gram-negative bacteria were tested in previous study [19]. Our data is consistent with the reported results, that the Et_3PAuCl is more effective than auranofin. Besides, it was reported that auranofin targets on Vfr, regulating *Pa*'s quorum sensing systems, type III secretion system (T3SS) and type IV pili (TFP) formation [16]. The active form of Me_3PAuCl is $[Au(PMe_3)]+$ which differs from the active form of auranofin/ Et_3PAuCl, $[Au(PEt_3)]+$, by replacing the ethyl-group with methyl-group. We speculated that Me_3PAuCl may showed higher suppression efficiency in inhibiting Vfr-regulated virulence mechanisms.

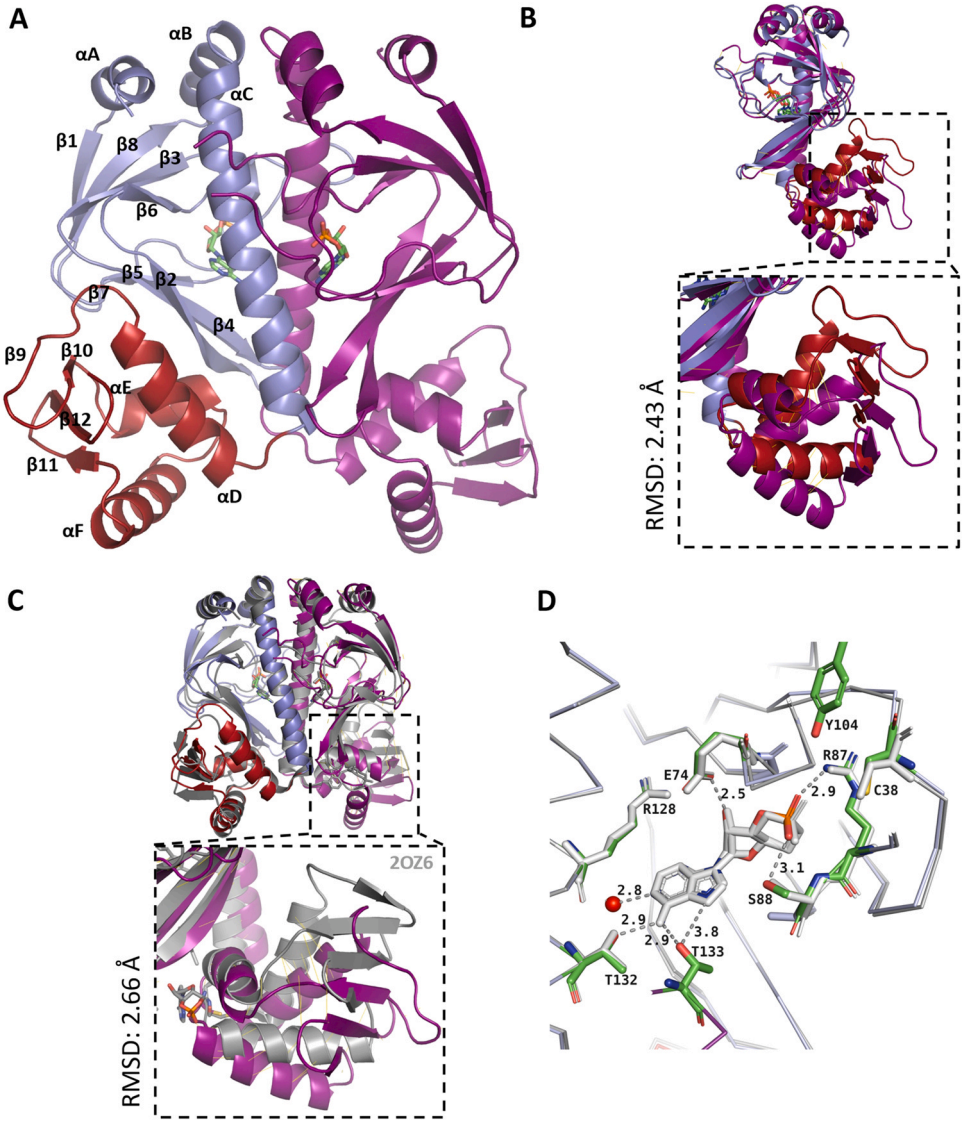

Fig. 3. Crystal structure of Vfr. (A) Annotated cartoon representation of Vfr dimer structure with the left monomer (Chain A) coloured in light blue for the ligand-binding N-terminal domain, in red for the DNA-binding C-terminal domain, and the cAMP ligand at the primary binding site is shown as sticks. Missing residues 80–84 in the right monomer (purple; Chain B) would cross in front of the left monomer. (B) Alignment of chains A and B, close-up insert highlights the difference in the C-terminal domain with a root mean square deviation (RMSD) of 2.43 Å over 162 backbone atoms. (C) Superimposition with Vfr bound with two cAMPs at both primary and secondary sites (PDB ID: 2OZ6; grey). Close-up insert distinguishes the asymmetric Chain B from its symmetric state in 2OZ6 with a root mean square deviation (RMSD) of 2.66 Å over 167 atoms. (D) Overlay with the primary cAMP-binding pocket of 2OZ6 (grey ribbon, including ligand and side chains), RMSD of 0.35 Å over 8 atoms. cAMP and neighboring residues are shown in stick representation (C, green; N, blue; O, red; P, orange; S, yellow), and water molecule is shown as a red sphere. Hydrogen bonds are represented by dashed lines and the corresponding interatomic distances are indicated.

2.2. Me_3PAuCl suppress Vfr-regulated virulence mechanism

We next examined whether Me_3PAuCl could inhibit Vfr-associated quorum sensing at a relatively low concentration with minimal effects on cell growth. We treated PAO1 wild-type strain by Me_3PAuCl at 0.2 μM (approximately at IC_{10} values of growth inhibition) and examined the dysregulated proteins by proteomic analysis. There were 154 proteins being dysregulated in response to Me_3PAuCl treatment, with 58 proteins being up-regulated and 96 being down-regulated (Table S2). As speculated, proteins involved in quorum sensing systems and biofilm formation were found suppressed in the presence of Me_3PAuCl (Fig. S1). When PAO1 was treated with Me_3PAuCl, expression of quorum sensing genes *lasB*, *rhlA* and *rhlB* were suppressed with fold change ratios of treated to control ($FC_{t/c}$) at 0.47 ± 0.03, 0.50 ± 0.03 and 0.42 ± 0.01, respectively. The *Pseudomonas* quinolone signal (PQS) system, *pqsBCDE* genes, which are responsible for the synthesis of PQS precursor, 2-Heptyl-4(1 H)-quinolone (HHQ), were also found suppressed in response to Me_3PAuCl, with $FC_{t/c}$ at 0.6 ± 0.01, 0.47 ± 0.01, 0.58 ± 0.01 and 0.58 ± 0.02, respectively. However, PqsH which convert HHQ to PQS only showed a slight suppression with $FC_{t/c}$ at 0.69 ± 0.02 with no statistical significance.

Furthermore, we evaluated QS inhibition efficiency of the Me_3PAuCl on PAO1 wild-type strain and PAO1 with overexpressed Vfr (Fig. 2). Me_3PAuCl was found to inhibit the expression of two major QS reporters LasB-GFP and RhlA-GFP with IC_{50} of 0.13 μM and 0.07 μM, respectively, in PAO1 strain (Fig. 2**A**). However, the overexpressed Vfr in PAO1 reduced the Me_3PAuCl sensitivity of *las* and *rhl* pathway, with increased IC_{50} of 0.324 μM and 0.254 μM, respectively (Fig. 2**B**). The QS-controlled virulence factors, elastase and pyocyanin, were down-regulated in the presence of a sub-lethal concentration of Me_3PAuCl (Fig. 2**C**). These observations are similar with the reported effects as auranofin on *P. aeruginosa*, that both auranofin and Me_3PAuCl cause reduced activities of QS and related

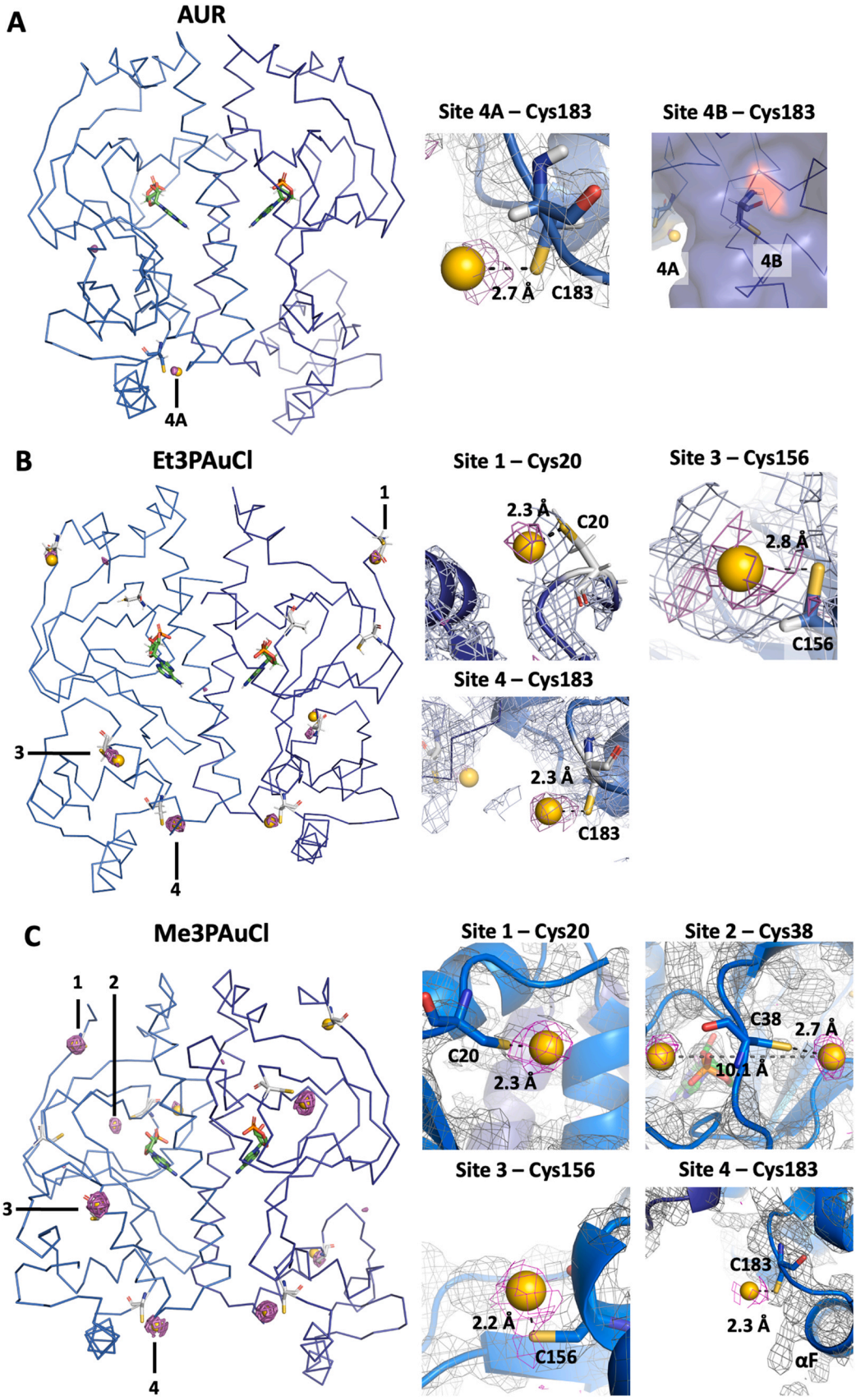

Fig. 4. Gold interacting sites of Vfr. Ribbon view of the overall structure (left) and the corresponding gold binding site numbered 1 – 4 with anomalous density peak of gold ions displayed as yellow spheres. The anomalous fourier map in the magenta mesh is contoured at a level of 4 σ with a mesh width of 4. Chain A is coloured in sky blue while chain B is in deep blue. Close-up cartoon view of potential gold binding sites (right) with the 2Fo-Fc map at a level of 1.0 σ in grey, and the anomalous density peak of gold ions contoured at a level of 3 σ. Hydrogen bonds are represented by dashed lines and the corresponding interatomic distances are indicated between the gold sphere and cysteine residue shown as stick. The surface view is displayed at 50 % transparency for the buried cysteine 183 site. (A) Auranofin condition which shows a weak anomalous peak at site 4. (B) Chloro (triethylphosphine)gold(I) found in all 4 sites except for site 2 of Chain A. (C) Chloro(trimethylphosphine)gold(I) found in all 4 sites.

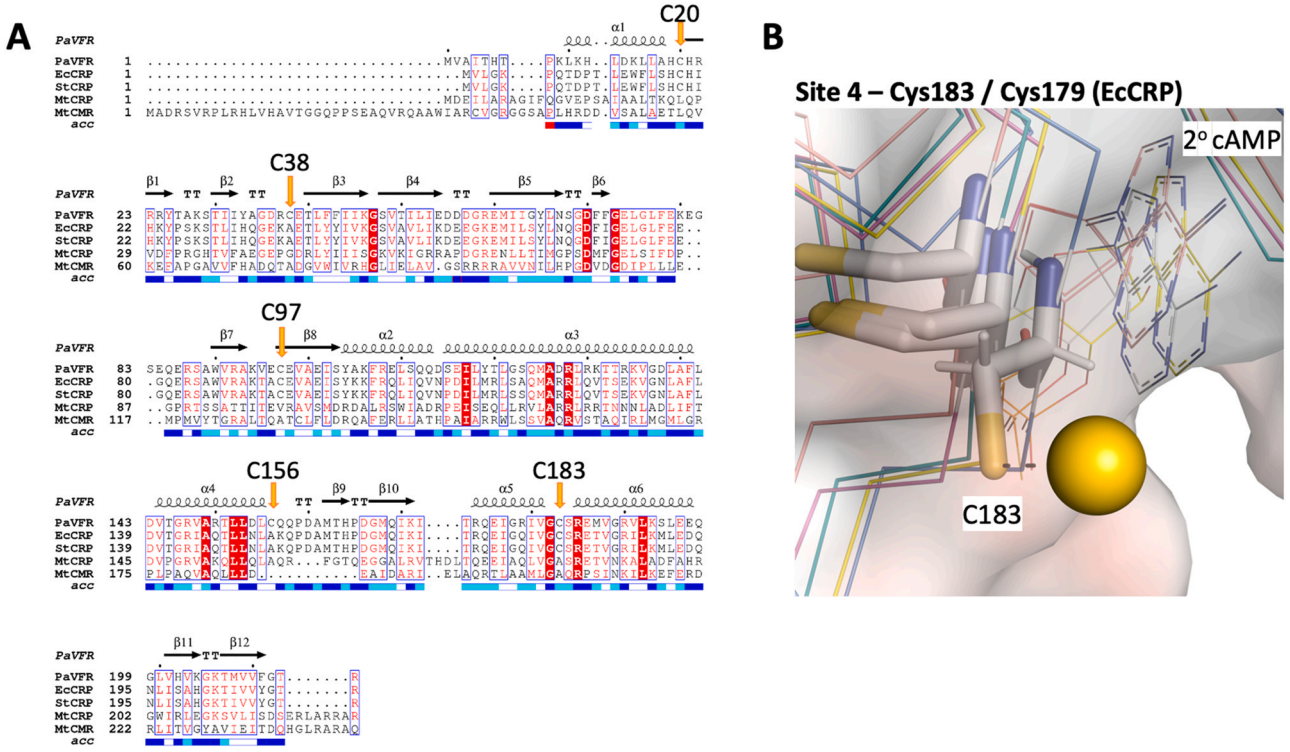

Fig. 5. Multiple sequence alignment of Vfr homologues and the corresponding superposition of the Cys183 site. (A) Multiple sequence alignment, red box with white characters represents strict identity, characters in red with blue frame represents 70 % similarity or higher across the group. Acc in the last row represents the relative accessibility of each residue with red as undetermined, blue for accessible, cyan for intermediate, and white as buried. (B) Ribbon view of backbone structure at Cys183 (gold binding site 4) with cAMP at secondary site displayed as lines. Vfr soaked with Et_3PAuCl (this study) is coloured in blue, Vfr bound to two cAMP (PDB ID: 2OZ6) in orange, *Ec*CRP bound to one cAMP (PDB ID: 1G6N) in purple, two cAMP (PDB ID: 4R8H) in teal, or with DNA (PDB ID: 2CGP) in yellow. Hydrogen bonds are represented by dashed lines and the gold atom as a sphere, with the corresponding cysteine residue shown as stick. Surface view is displayed at 50 % transparency.

phenotypes [16]. The auranofin can inhibits Vfr via its cysteine residues in vitro, though Vfr is not the only cellular target of auranofin. Interestingly, in our study, the elastase production was more sensitive to Me_3PAuCl at 1.0 μM in Vfr-over expressed system (Fig. 2**D**). This confirmed that Me_3PAuCl could effectively interact with Vfr, affecting its downstream gene expressions and regulations, although Vfr may not be the only target of Me_3PAuCl.

2.3. Auranofin and gold(I) analogues interact with Pa Vfr

The auranofin can inhibit Vfr via its free surface cysteine residues, as cysteine residue mutated Vfr is less regulated in the presence of auranofin [16]. Since Et_3PAuCl and Me_3PAuCl were shown to have much lower MIC and IC_{50} values, we hypothesize that these two compounds may be effective in interacting with the cysteines in Vfr. To test this hypothesis, we determined the crystal structures of *Pa* Vfr dimers bound to cAMP both alone and with the addition of gold compounds by means of soaking. We observed that there were no redox-active cysteine pairs and that the two monomers were bound with a cAMP ligand in the primary site (Fig. 3**A**). They formed an asymmetric dimer with a root mean square deviation (RMSD) of 2.43 Å over 162 backbone atoms largely due to the C-terminal domain (Fig. 3**B**). This differs from the prior Vfr structure with cAMP bound in both sites (PDB ID: 2OZ6) by Cordes et al. [5], where Vfr forms a symmetric dimer. Fig. 3**C** shows the overlay of 2OZ6 with our native structure, and the close-up insert highlights a similar significant conformational shift in the C-terminal domain with a RMSD of 2.66 Å over 167 atoms. 2OZ6 resembles the activated CRP-DNA (PDB ID: 2CGP) [20] as well as cAMP-bound CRP in both sites (PDB ID: 4R9H) [21], while our structures resemble the cAMP-bound CRP in the primary site (PDB ID: 1G6N) [22]. Hence our study suggests that the induced fit for DNA-binding by Vfr is similar to CRP. As expected, there is no difference for the primary cAMP binding pocket within the monomer (RMSD = 0.35 Å over 8 α-carbon pairs), and are formed by the same residues as shown in the superposed structures (Fig. 3**D**).

Au(I) binding is found in a linear-coordination at up to four of five available cysteine sites (Cys20, 38, 97, 156, and 183) within a distance of 2.8 Å. For auranofin, only one monomer (Chain A) was found bound to Au strongly at Cys183 (Site 4 A, Fig. 4**A**). While it would be expected for the two molecules to be the same in solution, the asymmetric Chain B Cys183 side chain is buried and inaccessible to bind to Au (Site 4B, Fig. 4**A**). This could be a crystal packing artifact that is not biologically meaningful. It is also possible that auranofin may bind to Chain B Cys183 and other Cys sites in solution (Table S3). In the case of Et_3PAuCl (Fig. 4**B**), the compounds were found to bound to cysteine sites 1 (Cys20), 3 (Cys156), and 4 (Cys183) in both chains. Similarly, in the case of Me_3PAuCl (Fig. 4**C**), a compound binding site was observed at 2 (Cys38), in addition to the sites identified for Et_3PAuCl. No significant conformational changes were observed with Au binding.

When compared with Vfr bound to two cAMP (PDB ID: 2OZ6), or in CRP bound to one cAMP (PDB ID: 1G6N), two cAMP (PDB ID: 4R8H), or with DNA (PDB ID: 2CGP), the sulfur group in Cys183 (Cys179 in CRP; Fig. 5**A**) is found buried and facing away from the secondary cAMP binding pocket (Fig. 5**B**). The sequence alignment between Vfr and CRP from *E. coli*, *Salmonella typhimurium*, and the distant *Mycobacterium tuberculosis* (Mt), showed that only Cys20 (site 1), Cys97 (inaccessible), and Cys183 (site 4) are the most conserved, except for *Mt*CRP and *Mt*CMR, and further emphasized the importance of site 4 (Fig. 5**A**). The inhibition by gold interferes with DNA binding at the C-terminal domain (Fig. 6**, Left**), where gold at site 4 would clash with the DNA backbone binding at positions 9 and 10 of the primary kink (PDB ID: 1ZRC) [23] and site 3 would affect

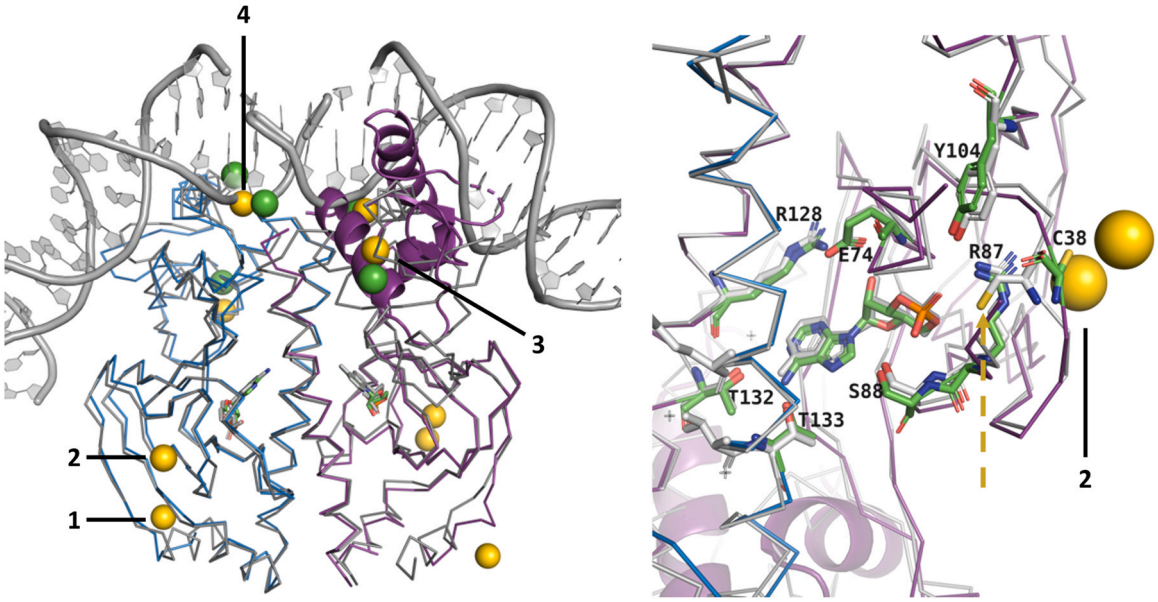

Fig. 6. The influence of gold binding sites on Vfr structure. (Left) Ribbon model overlay of the DNA-bound CRP structure (PDB ID: 1ZRC; in grey for all atoms) on Me_3PAuCl-bound Vfr (blue for Chain A, and purple for Chain B), with gold and chloride ions displayed as gold and green spheres respectively, and cAMP ligands as stick (C, green; N, blue; O, red; P, orange; S, yellow). The C-terminal domain of Chain B is shown in the cartoon (purple) to highlight its incompatible conformation for DNA-binding. (Right) Close-up of the primary cAMP binding pocket overlay between Me_3PAuCl-bound Vfr (same colour scheme as in Left panel) with the symmetric Vfr structure (PDB ID: 2OZ6) in grey where the gold binding site 2 is found. There are two gold spheres with both having 0.5 occupancies. The yellow dashed arrow highlights the sulphur group of C38 in the Vfr structure (grey).

domain reorientation from asymmetric to symmetric state. Furthermore, another gold binding at site 2 would alter the primary cAMP binding pocket (Fig. 6**, right**). The presence of the gold compound at site 4 (C-terminal domain of Chain A) clashes with the DNA backbone, suggesting a mechanism of transcription inhibition (Fig. 6**, left**). Furthermore, the C-terminal domain of Chain B is also incompatible with conformation for DNA-binding. The gold at site 3 would also interfere with the shift required to the symmetric form. We also show that the gold binding causes the cysteine sulphur residue to face outwards, away from the cAMP ligand as indicated by the yellow arrow of the original location, hence altering the binding site (Fig. 6**, right**). Overall, the number of sites with gold compound binding found in the structural study correlates with the IC_{50} (Fig. 1) whereby Me_3PAuCl (4 sites) is the most potent followed by Et_3PAuCl (3 sites) and Auranofin (1 site), respectively.

3. Conclusion

Gold therapy, also known as Chryso- or aurotherapy, has been of interest since its discovery in traditional to modern medicine, with growing insights into their molecular targets, applications, and know-how towards more targeted delivery [24,25]. While auranofin has declined in its original use for rheumatoid arthritis due to new alternatives with fewer side effects from long-term usage, the wide-ranging repurposed applications as an anti-cancer drug and a broad-spectrum antibiotic underscore the importance of our study herein. We have provided mechanistic insights of Vfr inhibition by auranofin and related gold compounds. Our findings reveal that the cysteine residues of cAMP transcription factors are free to rotate, which supports the model of the biphasic cAMP concentration dependence activity [20].

Auranofin has low resistance potential due to the multiple targets of gold compounds, making it a candidate for use in combination with antibiotics such as colistin which is a last resort treatment for *Pa* and other gram negatives [14,16]. However, auranofin's limitation include accumulation in cells and decreased effectiveness compared to Et_3PAuCl and Me_3PAuCl, as demonstrated in our study by 3- to10-fold difference. This not only limits its clinical use but also raises concerns about its toxicity. The use of simpler and more potent gold-phosphine compound, Me_3PAuCl, with similar biological and pharmacological properties may overcome these limitations. Given that they lead to more severe bowel irritation [24], recent work on encapsulating these active ingredients in biocompatible nanoparticles [26] points an approach forward to expedite their clinical use for *Pa* infections.

4. Experimental procedures

4.1. Chemicals and bacterial strains

Auranofin, Et_3PAuCl, and Me_3PAuCl were purchased from Sigma (product codes A6733, 404217, and 288225, respectively). Stock solutions of 100 mM were prepared in DMSO (Sigma, D8418). *P. aeruginosa* PAO1 was used as model organism for all experiments. Luria-Bertani (LB) broth (1 % tryptone and 0.5 % yeast extract), Mueller Hinton broth (MHB), and ABTGC [27] (AB minimal medium supplemented with 0.2 % glucose and 0.2 % casamino acids) and agar were used to grow bacterial cultures and/or biological assays.

4.2. Expression and purification of Vfr

Coding sequence with 5N-terminal amino acid truncation of Vfr (Vfr-Ndel5) from PAO1 was inserted into pSUMO-LIC vector flanked by an N-terminus His6-SUMO affinity tag and protease site via ligation-independent cloning (LIC) cloning (NTU Protein Production Platform; PPP). Vfr was overexpressed from pSUMO-LIC-*vfr* in *Escherichia coli* strain Rosetta T1R (DE3) cells when OD600 reaches 0.8–1.0 in LB and induced with 1 mM IPTG overnight at 18 °C. The harvested cell pellet was resuspended in Buffer A1 (300 mM NaCl, 50 mM Tris-HCL pH 7.5, 20 mM imidazole, 4 mM 2-Mercaptoethanol, 10 % Glycerol), lysed using a homogenizer and the cell debris removed via centrifugation at 40,000 x g. The supernatant was loaded to a HisFF HP column (Cytiva, Marlborough, MA, USA) and eluted with a 20–300 mM imidazole linear gradient. The eluted proteins were further diluted to a salt concentration of 100 mM before the addition of SUMO protease and 2 mM cAMP (Sigma, A6885) and

dialysed against Buffer A2 (100 mM NaCl, 50 mM Tris-HCL pH 7.5, 4 mM 2-Mercaptoethanol, 5 % Glycerol) for 3 h. This was then applied to a HiTrap Heparin FF (Cytiva) and eluted with a 100–1000 mM gradient of NaCl linear gradient. The Vfr-containing fractions were then concentrated using a 10 kDa MWCO spin concentrator (Vivaspin; Sartorius, Göttingen, Germany) before loading on a HiLoad 26/60 Superdex 200 pg (Cytiva) column equilibrated with Buffer A3 (300 mM NaCl, 25 mM HEPES pH 7.5, 1 mM TCEP, 5 % Glycerol). Pooled peak fractions were concentrated to 23 mg/mL, flash frozen in liquid nitrogen, and stored at −80 °C until their use. Protein concentrations were determined by using Protein Assay Dye (Bio-Rad, California, USA).

4.3. Crystallization, data collection, and structure determination

Prior to crystallization, Vfr was first diluted to 10 mg/mL in 300 mM NaCl, 25 mM HEPES pH 7.5, 5 % glycerol and 2 mM cAMP. Crystals were grown by vapor diffusion from hanging drops containing a 1:1 ratio of Vfr at 6 mg/mL and a good solution of 2.6 M Ammonium Sulphate and 0.1 M Bicine pH 9.0 in 24-well plates. Crystals were dehydrated overnight and flash frozen in liquid nitrogen in the same crystallization condition supplemented with 19 % glycerol before mounting. For vfr-inhibitor cocrystals, vfr crystals were soaked with 1.25 mM inhibitor dissolved in 2.5 % DMSO, 2.6 M Ammonium Sulphate, 0.1 M Bicine pH 9.0 supplemented with 18 % glycerol. Diffraction data were collected at home source (Rigaku FR-X and Dectris Pilatus3R 300 K detector), and at beamlines TPS05A and BL15A1 of National Synchrotron Radiation Research Center (Hsinchu, Taiwan; proposal no. 2019–1–135–2), and the MX1 of the Australian Synchrotron, ANSTO (Victoria, Australia; proposal no. 14981b). Data indexing and integration were done using either iMOSFLM [28] or HKL-3000 [29]. Scaling and merging of the intensities were carried out using POINTLESS and AIMLESS from CCP4 suite [30]. The crystals belong to space group C 1 2 1, except crystals soaked in Chloro(trimethylphosphine)gold(I) which resulted in the space group P1 instead. Initial phases were determined by molecular replacement using Vfr structure (PDB ID 2OZ6) as the search model using either Molrep [31] or Phaser [32]. Subsequent iterative rounds of refinement were done using the Phenix.refine program [33,34] and manual rebuilding using Coot [35]. The twin law (h,h-k,h-l) was applied for Vfr crystals soaked with Chloro(trimethylphosphine)gold (I) during Phenix refinement to correct for twining effects. Disordered regions in the N-terminal, between residues 80 – 84, and the C-terminal were excluded in the final models. The locations of gold atoms were defined using the anomalous Fourier maps. Atomic coordinates and structure factors of Vfr with cAMP only, auranofin, Et_3PAuCl, and Me_3PAuCl, have been deposited in the Protein Data Bank with the accession codes 7FEW, 7FF0, 7FF8, and 7FF9 respectively. Figures were generated using Pymol [36]. Data collection and refinement statistics are summarized in Table S2.

4.4. Sequence alignment and analysis

Vfr (Uniprot ID P55222) and related homologous sequences, EcCRP (Uniprot ID P0ACJ8), StCRP (Uniprot ID P0A2T6), MtCRP (Uniprot ID: P9WMH3), and MtCMR (EcCRP (Uniprot ID P9WMH5), were curated from the non-redundant sequence database and literature review. The alignment was carried out using MUSCLE program [37] in MEGA X [38] and visualized using ESPript3.0 on ENDscript server (ESPript - https://espript.ibcp.fr) [39] for structural feature annotation and the residue relative accessibility.

4.5. Elastase assay

P. aeruginosa PAO1 wild type and PAO1::*vfr* were cultivated in LB medium overnight at 37 °C with shaking, and were adjusted to the concentration of OD600 at 1.0; respectively. The bacterial suspension was inoculated into ABTGC containing 1 μM Me_3PAuCl or DMSO at a ratio of 1:1000 *v*:*v* and was cultivated at 37 °C with shaking for 18 h. The gold-compound treated cultures and control were diluted to approximately 1×10^6 CFU/mL, and 3 μL diluted suspension was doted in Skim Milk Medium for overnight cultivation at 37 °C. Plate images were visualized by G-BOX Chemi XT 4 (Genesys version 1.3.4.0, Syngene).

4.6. Pyocyanin assay

Pyocyanin production by PAO1 and PAO1::*vfr* was measured as described previously [40]. In brief, overnight bacterial culture was diluted to 1×10^6 CFU/mL in ABTGC containing 1 μM Me_3PAuCl or DMSO, and cultivated at 37 °C with shaking for 24 h. The bacterial culture was centrifuged at 8000 g for 10 min to collect the supernatant. Chloroform (1.2 mL) was added to the supernatant and was vortexed vigorously. The chloroform layer was carefully collected, followed by re-extraction with 400 μL of 0.2 M HCl. The HCl layer was carefully after centrifugation at 4500 rpm for 10 min at 4 ℃ with absorbance measured at OD_{380} against 0.2 M HCl.

4.7. Growth inhibition assay

The minimum inhibitory concentration (MIC) of gold compounds against *P. aeruginosa* PAO1 was determined in a standard broth dilution assay. PAO1was grown overnight (~18 h) in LB at 37 °C with orbital shaking (180 rpm), which was adjusted to a concentration of OD_{600} at 1 before inoculation. Serial two-fold dilutions of gold compounds were prepared from DMSO stock solutions in ABTGC medium. The bacterial suspension was inoculated into ABTGC medium containing gold compounds/DMSO at a concentration of OD_{600} at 0.01 and was cultivated at 37 °C with shaking for 18 h. Assays were repeated three times with triplicate each batch on different days. Growth curve was plotted for each compound's each dosing concentration. Here we utilize IC_{90} to represent the MIC for each compound. The media turbidity of bacterial culture at early stationary growth stage (10 h) under the treatment of each concentration for each gold compound were plotted. IC_{90} and IC_{50} values for each compound were calculated by nonlinear regression curve fitting. The MIC of gold compounds against PAO1 in MHB medium was assessed using the same protocol, with the substitution of ABTGC with MHB.

4.8. Proteomics analysis

The proteomics analysis was conducted following the reported procedures [16]. In brief, PAO1was grown overnight (~18 h) in LB at 37 °C with orbital shaking (180 rpm), which was adjusted to a concentration of OD_{600} at 1 before inoculation. The bacterial suspension was inoculated into ABTGC medium containing gold compounds/DMSO at a concentration of OD_{600} at 0.01 and was cultivated at 37 °C with shaking for 10 h. Then, bacterial cells were harvested and the cell pellets were washed twice with 1x PBS buffer, followed by being resuspended in 2 mL lysis buffer containing 0.5 M triethylammonium bicarbonate (TEAB), 0.1 M SDS and protease inhibitor cocktail (Sigma-Aldrich, USA). The cells were lysed using probe sonication at 30 % amplitude for 5 min (10 s intervals for each 10 s sonication). The soluble proteins were collected by centrifugation at 4 °C at 16,000 g for 20 min to discard the cell debris. 200 μg proteins for each sample were denatured and concentrated using 2D-SDS-PAGE. Gel fragments were submitted for TMT proteomics analysis by QL Bio (www.qinglianbio.com, Beijing, China).

4.9. Statistical analysis

All statistical tests were performed with GraphPad Prism (V9, GraphPad, USA). P-values of < 0.05 were considered significant. The student's t-test was used to evaluate the growth and QS inhibition of gold compounds on PAO1, motility and other phenotypic assays.

Funding

This research is supported by the Singapore Ministry of Education under its Singapore Ministry of Education Academic Research Fund Tier 1 (2018-T1-002-010) and Tier 2 (2016-T2-2-097) to D.L.; Nanyang Presidential Graduate Scholarship to B.L.A.C.; the Guangdong Natural Science Foundation for Distinguished Young Scholar [2020B1515020003]; the National Key Research and Development Program of China (2022YFC2304700); the National Natural Science Foundation of China (32270196 and 32200155); the Guangdong Basic and Applied Basic Research Foundation [2019A1515110640]; and the Shenzhen Overseas High-level Talent Team (KQTD20200909113758004).

CRediT authorship contribution statement

Liang, Y. and Luo, D. conceived and designed the experiments. Chew, B.L.A. performed the structural studies and wrote the first draft of the manuscript. Chew, B.L.A. and Luo, D. analyzed and prepared the structural figures. Wang, J. performed the bacterial assays. Wang, J. and Zhang, Y. analyzed the biological results and revised the manuscript. All authors participated in the writing of the manuscript.

Declaration of Competing Interest

No conflict of interest exists in the submission of this manuscript, and all authors have gone through the manuscript and approved to submit to your journal. I would like to declare on behalf of my co-authors that the work described was original research that has not been published previously, and is not under consideration for publication elsewhere, in whole or in part.

L.Y. is part of the international patent (WO2017044044A1, filed 6th September 2016) related to the work described in this manuscript.

Acknowledgments

We gratefully acknowledge the beamline staff at TPS 05A beamline at the National Synchrotron Radiation Research Center (Hsinchu, Taiwan), MXII beamline at the Australian Light Source (Melbourne, Australia), and PSIII beamline in Swiss Light Source (SLS; Paul Scherrer Institut, Switzerland) for providing us with outstanding support during data collection. We are also thankful to Dr. Ruslan Sanishvili and Dr. Leela Ruckthong for organizing the SEA COAST 2019 workshop where we received expert help from Mr. Ronan Keegan and Dr. Garib Murshudov in resolving issues with the Auranofin dataset collected at home source.

Appendix A. Supporting information

Supplementary data associated with this article can be found in the online version at doi:10.1016/j.csbj.2023.03.013.

References

[1] CDC. Antibiotic Resistance Threats in the United States CDC. Atlanta, GA: U.S. Department of Health and Human Services; 2019.
[2] Tacconelli E, Carrara E, Savoldi A, Harbarth S, Mendelson M, Monnet DL, et al. Discovery, research, and development of new antibiotics: the WHO priority list of antibiotic-resistant bacteria and tuberculosis. Lancet Infect Dis 2018;18:318–27. https://doi.org/10.1016/s1473-3099(17)30753-3
[3] Suh S-J, Runyen-Janecky LJ, Maleniak TC, Hager P, MacGregor CH, Zielinski-Mozny NA, et al. Effect of vfr mutation on global gene expression and catabolite repression control of Pseudomonas aeruginosa. Microbiology 2002;148:1561–9. https://doi.org/10.1099/00221287-148-5-1561
[4] Frendorf PO, Lauritsen I, Sekowska A, Danchin A, Norholm MHH. Mutations in the global transcription factor CRP/CAP: insights from experimental evolution and deep sequencing. Comput Struct Biotechnol J 2019;17:730–6. https://doi.org/10.1016/j.csbj.2019.05.009
[5] Cordes TJ, Worzalla GA, Ginster AM, Forest KT. Crystal structure of the Pseudomonas aeruginosa virulence factor regulator. J Bacteriol 2011;193:4069–74. https://doi.org/10.1128/JB.00666-10
[6] West SE, Sample AK, Runyen-Janecky LJ. The vfr gene product, required for Pseudomonas aeruginosa exotoxin A and protease production, belongs to the cyclic AMP receptor protein family. J Bacteriol 1994;176:7532–42. https://doi.org/10.1128/jb.176.24.7532-7542.1994
[7] Coggan KA, Wolfgang MC. Global regulatory pathways and cross-talk control pseudomonas aeruginosa environmental lifestyle and virulence phenotype. Curr Issues Mol Biol 2012;14:47–70.
[8] Albus AM, Pesci EC, Runyen-Janecky LJ, West SE, Iglewski BH. Vfr controls quorum sensing in Pseudomonas aeruginosa. J Bacteriol 1997;179:3928–35. https://doi.org/10.1128/jb.179.12.3928-3935.1997
[9] Kamath S, Kapatral V, Chakrabarty AM. Cellular function of elastase in Pseudomonas aeruginosa: role in the cleavage of nucleoside diphosphate kinase and in alginate synthesis. Mol Microbiol 1998;30:933–41. https://doi.org/10.1046/j.1365-2958.1998.01121.x
[10] Zhang Y, Zhang C, Du X, Zhou Y, Kong W, Lau GW, et al. Glutathione Activates Type III Secretion System Through Vfr in Pseudomonas aeruginosa. Front Cell Infect Microbiol 2019;9:164. https://doi.org/10.3389/fcimb.2019.00164
[11] Davinic M, Carty NL, Colmer-Hamood JA, San Francisco M, Hamood AN. Role of Vfr in regulating exotoxin A production by Pseudomonas aeruginosa. Microbiol (Read) 2009;155:2265–73. https://doi.org/10.1099/mic.0.028373-0
[12] Beatson SA, Whitchurch CB, Sargent JL, Levesque RC, Mattick JS. Differential regulation of twitching motility and elastase production by Vfr in Pseudomonas aeruginosa. J Bacteriol 2002;184:3605–13. https://doi.org/10.1128/JB.184.13.3605-3613.2002
[13] Jang HI, Eom YB. Repurposing auranofin to combat uropathogenic Escherichia coli biofilms. J Appl Microbiol 2019;127:459–71. https://doi.org/10.1111/jam.14312
[14] Sun H, Zhang Q, Wang R, Wang H, Wong YT, Wang M, et al. Resensitizing carbapenem- and colistin-resistant bacteria to antibiotics using auranofin. Nat Commun 2020;11:5263. https://doi.org/10.1038/s41467-020-18939-y
[15] Diez-Martinez R, Garcia-Fernandez E, Manzano M, Martinez A, Domenech M, Vallet-Regi M, et al. Auranofin-loaded nanoparticles as a new therapeutic tool to fight streptococcal infections. Sci Rep 2016;6:19525. https://doi.org/10.1038/srep19525
[16] Yam JKH, Tan LZW, Hong Z, Salido MMS, Woo BY, Yong AMH, et al. Auranofin inhibits virulence pathways in Pseudomonas aeruginosa. Bioorg Med Chem 2023;79:117167. https://doi.org/10.1016/j.bmc.2023.117167
[17] Barry NP, Sadler PJ. Exploration of the medical periodic table: towards new targets. Chem Commun (Camb) 2013;49:5106–31. https://doi.org/10.1039/c3cc41143e
[18] Cirri D, Bartoli F, Pratesi A, Baglini E, Barresi E, Marzo T. Strategies for the improvement of metal-based chemotherapeutic treatments. Biomedicines 2021;9. https://doi.org/10.3390/biomedicines9050504
[19] Marzo T, Cirri D, Pollini S, Prato M, Fallani S, Cassetta MI, et al. Auranofin and its analogues show potent antimicrobial activity against multidrug-resistant pathogens: structure-activity relationships. ChemMedChem 2018;13:2448–54. https://doi.org/10.1002/cmdc.201800498
[20] Passner JM, Steitz TA. The structure of a CAP–DNA complex having two cAMP molecules bound to each monomer. Proc Natl Acad Sci 1997;94:2843–7. https://doi.org/10.1073/pnas.94.7.2843
[21] Townsend PD, Rodgers TL, Glover LC, Korhonen HJ, Richards SA, Colwell LJ, et al. The role of protein-ligand contacts in allosteric regulation of the Escherichia coli catabolite activator protein. J Biol Chem 2015;290:22225–35. https://doi.org/10.1074/jbc.M115.669267
[22] Passner JM, Schultz SC, Steitz TA. Modeling the cAMP-induced allosteric transition using the crystal structure of CAP-cAMP at 2.1 A resolution. J Mol Biol 2000;304:847–59. https://doi.org/10.1006/jmbi.2000.4231
[23] Napoli AA, Lawson CL, Ebright RH, Berman HM. Indirect readout of DNA sequence at the primary-kink site in the CAP-DNA complex: recognition of pyrimidine-purine and purine-purine steps. J Mol Biol 2006;357:173–83. https://doi.org/10.1016/j.jmb.2005.12.051
[24] Parish RV. Gold in medicine - chrysotherapy. Interdiscip Sci Rev 1992;17:221–8. https://doi.org/10.1179/isr.1992.17.3.221
[25] Roder C, Thomson MJ. Auranofin: repurposing an old drug for a golden new age. Drugs R D 2015;15:13–20. https://doi.org/10.1007/s40268–015-0083-y
[26] Menconi A, Marzo T, Massai L, Pratesi A, Severi M, Petroni G, et al. Anticancer effects against colorectal cancer models of chloro(triethylphosphine)gold(I) encapsulated in PLGA-PEG nanoparticles. Biometals 2021. https://doi.org/10.1007/s10534-021-00313-0
[27] Tan SY, Chua SL, Chen Y, Rice SA, Kjelleberg S, Nielsen TE, et al. Identification of five structurally unrelated quorum-sensing inhibitors of Pseudomonas

aeruginosa from a natural-derivative database. Antimicrob Agents Chemother 2013;57:5629–41. https://doi.org/10.1128/AAC.00955-13
[28] Battye TGG, Kontogiannis L, Johnson O, Powell HR, Leslie AGW. iMOSFLM: a new graphical interface for diffraction-image processing withMOSFLM. Acta Crystallogr Sect D Biol Crystallogr 2011;67:271–81. https://doi.org/10.1107/s0907444910048675
[29] Minor W, Cymborowski M, Otwinowski Z, Chruszcz M. HKL-3000: the integration of data reduction and structure solution - from diffraction images to an initial model in minutes. Acta Crystallogr Sect D 2006;62:859–66. https://doi.org/10.1107/S0907444906019949
[30] Winn MD, Ballard CC, Cowtan KD, Dodson EJ, Emsley P, Evans PR, et al. Overview of theCCP4 suite and current developments. Acta Crystallogr Sect D Biol Crystallogr 2011;67:235–42. https://doi.org/10.1107/s0907444910045749
[31] Vagin A, Teplyakov A. Molecular replacement with MOLREP. Acta Crystallogr D Biol Crystallogr 2010;66:22–5. https://doi.org/10.1107/s0907444909042589
[32] McCoy AJ, Grosse-Kunstleve RW, Adams PD, Winn MD, Storoni LC, Read RJ. Phaser crystallographic software. J Appl Crystallogr 2007;40:658–74. https://doi.org/10.1107/S0021889807021206
[33] Afonine PV, Grosse-Kunstleve RW, Echols N, Headd JJ, Moriarty NW, Mustyakimov M, et al. Towards automated crystallographic structure refinement with phenix.refine. Acta Crystallogr Sect D 2012;68:352–67. https://doi.org/10.1107/S0907444912001308
[34] Adams PD, Afonine PV, Bunkoczi G, Chen VB, Davis IW, Echols N, et al. PHENIX: a comprehensive Python-based system for macromolecular structure solution. Acta Crystallogr Sect D 2010;66:213–21. https://doi.org/10.1107/S0907444909052925
[35] Emsley P, Lohkamp B, Scott WG, Cowtan K. Features and development of Coot. Acta Crystallogr Sect D Biol Crystallogr 2010;66:486–501. https://doi.org/10.1107/s0907444910007493
[36] Schrodinger, L.L.C. (2015) The PyMOL Molecular Graphics System, Version 1.8.
[37] Edgar RC. MUSCLE: a multiple sequence alignment method with reduced time and space complexity. BMC Bioinforma 2004;5:113. https://doi.org/10.1186/1471-2105-5-113
[38] Stecher G, Tamura K, Kumar S. Molecular Evolutionary Genetics Analysis (MEGA) for macOS. Mol Biol Evol 2020;37:1237–9. https://doi.org/10.1093/molbev/msz312
[39] Robert X, Gouet P. Deciphering key features in protein structures with the new ENDscript server. Nucleic Acids Res 2014;42:W320–4. https://doi.org/10.1093/nar/gku316
[40] Jantaruk P, Pabuprapap W, Nakaew A, Kunthalert D, Suksamrarn A. 4-methoxybenzalacetone, the cinnamic acid analog as a potential quorum sensing inhibitor against Chromobacterium violaceum and Pseudomonas aeruginosa. World J Microbiol Biotechnol 2021;37:153. https://doi.org/10.1007/s11274-021-03119-x